Acta Crystallographica Section B
Structural Science
ISSN 0108-7681

Terephthalate salts of dipositive cations

James A. Kaduk

BP Chemicals, PO Box 3011 MC F-9, Naperville, IL 60566, USA

Correspondence e-mail: kadukja@bp.com

Received 13 December 2001
Accepted 20 May 2002

The crystal structures of $M(C_8H_4O_4)(H_2O)_2$, M = Mg, Mn, Fe and Co, have been determined by applying Monte Carlo simulated annealing techniques to synchrotron powder diffraction data and refined by the Rietveld method using both synchrotron and laboratory powder data. These isostructural compounds crystallize in the monoclinic space group $C2/c$, with $18.2734\ (9) \leq a \leq 18.7213\ (13)$, $6.5186\ (13) \leq b \leq 6.5960\ (4)$, $7.2968 \leq c \leq 7.4034\ (6)$ Å, $98.653\ (2) \leq \beta \leq 99.675\ (1)^\circ$ and $Z = 4$. The structure consists of alternating layers (perpendicular to a) of terephthalate anions and octahedrally coordinated metal cations. The octahedra are isolated; each carboxylate bridges two metal cations. The equatorial metal coordination consists of four terephthalate O atoms and there are two axial water molecules. Both water-molecule H atoms participate in normal-strength hydrogen bonds to carboxylate O atoms. Quantum chemical calculations (using *CASTEP*) were used to determine the H-atom positions and analyze the hydrogen bonding and the metal coordination. Both the atomic charges and the M—O bond-overlap populations indicate that, despite the fact that these compounds are isostructural, the metal–terephthalate bonding is different. The bonding in the Mg complex is essentially ionic, while the M—O bonds in the Mn, Fe and Co complexes have significant covalent character. Comparison of a new Rietveld refinement of the structure of copper(II) terephthalate trihydrate with the reported single-crystal structure provides an opportunity to assess the accuracy and precision that can be expected from structures of aromatic carboxylates determined using X-ray powder data. The average difference between the bond distances in the two structures is 0.03 Å and the average difference in bond angles is only 1.1°.

1. Introduction

Purified terephthalic acid (PTA, 1,4-benzenedicarboxylic acid) is the primary and preferred raw material for the polyester used to make a myriad of consumer and industrial products. BP Chemicals technology produces over 3×10^9 kg of PTA per year. A feed mix of *p*-xylene, catalyst and acetic acid is oxidized with air in a continuous homogeneous reactor, where crude terephthalic acid (TA) is produced (Barker & Saffer, 1958; Partenheimer, 1995). Purified terephthalic acid is then obtained through heterogeneous catalytic hydrogenation and crystallization (Meyer, 1971). From time to time, terephthalate salts are isolated from process streams. Understanding the natures of terephthalate complexes of catalyst and corrosion metals should lead to process insights and improvements.

Little is known about the solid-state structures of terephthalate salts. Powder diffraction data have been reported for several metal terephthalates (Sherif, 1970) and the prepara-

tions of others have been described (Brzyska, 1971). Only the structures of zinc terephthalate dihydrate (Guilera & Steed, 1999; CSD Refcode DIKQET), copper terephthalate dihydrate (Deakin *et al.*, 1999; CSD Refcode KEQTEF), copper terephthalate trihydrate (Cueto *et al.*, 1991; CSD Refcode JIBFUV; Deakin *et al.*, 1999; CSD Refcode JIBFUV01), triaquaterephthalatocadmium tetrahydrate (Michaelides *et al.*, 1998; CSD Refcode SAQYEO), calcium terephthalate trihydrate (Matsuzaki & Iitaka, 1972; CSD Refcode CATPAL; Groeneman & Atwood, 1999; CSD Refcode CATPAL01), strontium terephthalate tetrahydrate, barium terephthalate tetrahydrate (Groeneman & Atwood, 1999; CSD Refcodes LOCCAH, LOCCEL), barium terephthalate (Miyakubo *et al.*, 1994; CSD Refcode ZEFNIH), diterbium tris(terephthalate) tetrahydrate (Reineke *et al.*, 1999; CSD Refcode QACTUJ), dilithium terephthalate (Kaduk, 2000; CSD Refcode MAQDUD), disodium terephthalate (Furuyama & Ebara, 1967; CSD Refcode QQQDHD; Kaduk, 2000; CSD Refcode QQQDHD01), dipotassium terephthalate (Ebara & Furuyama, 1973; CSD Refcode PTRPHT; Furuyama & Ebara, 1967; Kaduk, 2000; CSD Refcode PTRPHT02) and diammonium terephthalate (Kaduk, 2000) have been reported.

Most of the terephthalates isolated from commercial operations are intractable solids and consist of mixtures of compounds. We have undertaken a program to prepare pure materials and understand the solid-state structures of aromatic carboxylates, particularly terephthalates. The crystal structures of magnesium, manganese, iron and cobalt terephthalate dihydrates provide valuable 'intellectual capital' for the characterization of plant deposits. Comparison of the Rietveld-refined structure of copper terephthalate trihydrate with the reported single-crystal structure provides insight into the accuracy of such structures determined using powder data.

2. Experimental

2.1. Magnesium terephthalate dihydrate

A solution of 0.5242 g of $(NH_4)_2C_8H_4O_4$ in 30 ml of water was filtered to remove trace insoluble impurities, mixed with a solution of 0.5732 g of $Mg(C_2H_3O_2)(H_2O)_4$ in 20 ml of water and heated at 373 K until the volume had decreased to about 20 ml. The slurry was filtered hot, washed with water and ethanol, and air-dried to yield 0.1116 g of white powder.

2.2. Manganese terephthalate dihydrate

A solution of 1.0080 g of $(NH_4)_2C_8H_4O_4$ in 60 ml of water was filtered to remove a trace of insoluble material. A solution of 1.4578 g of $Mn(C_2H_3O_2)_2(H_2O)_4$ in 40 ml of water was added slowly with stirring. The solution was stirred at room temperature for 30 min, during which time a white precipitate formed. The slurry was filtered, washed with water and air-dried. The yield was 0.788 g. A preliminary powder pattern indicated that this solid was a mixture. A portion of the solid was slurried with water at 353 K overnight to yield phase-pure $Mn(C_8H_4O_4)(H_2O)_2$.

2.3. Iron terephthalate dihydrate

25.0 g of $K_2C_8H_4O_4$ was dissolved in 400 ml of de-gassed water in a 1000 ml three-necked flask under a nitrogen purge. To this solution was added a solution of $FeCl_2(H_2O)_4$ in 200 ml of de-gassed water, over the course of about 20 min. The 23.1 g of canary-yellow solid were filtered under a nitrogen purge and dried in a vacuum oven overnight at room temperature. The solid is not stable on long-term storage in the atmosphere.

2.4. Cobalt terephthalate dihydrate

Cobalt terephthalate dihydrate was prepared by the method of Sherif (1970). At temperatures much above ambient, the pink solid begins to decompose.

2.5. Copper terephthalate trihydrate

A solution of 1.0103 g of $(NH_4)_2C_8H_4O_4$ in 50 ml of water was frozen with liquid nitrogen. A solution of 0.9952 g of $Cu(C_2H_3O_2)_2(H_2O)$ in 40 ml of water was layered on top. The frozen layers were allowed to warm to room temperature overnight. The slurry was filtered, washed with water and ethanol, and air-dried to yield 1.166 g of blue solid.

2.6. Powder diffraction data

Powder patterns of magnesium terephthalate dihydrate were measured from 1 mm capillary specimens at both the MRCAT ID10 beamline at the Advanced Photon Source (6–37.125° 2θ, 0.005° steps, 0.5 s per step, $\lambda = 1.0331$ Å) and beamline X3B1 at the National Synchrotron Light Source (7–55° 2θ, 0.005° steps, 1 s per step, $\lambda = 1.149896$ Å). Laboratory powder patterns of the Mg, Mn, Fe, Co and Cu salts (see supplementary material)[1] were measured from flat-plate specimens on a Scintag PAD V diffractometer equipped with an Ortec intrinsic Ge detector using Cu $K\alpha$ radiation.

2.7. Structure solution

The synchrotron patterns of magnesium terephthalate could be indexed on a *C*-centered monoclinic unit cell having $a = 18.511$, $b = 6.536$, $c = 7.317$ Å, $\beta = 99.734°$ and $V = 872.5$ Å^3. The systematic absences were consistent with space groups $C2/c$ or Cc. To obtain a reasonable density, $Z = 4$. Space group $C2/c$ was selected and confirmed by successful solution and refinement of the structures. A terephthalate anion was built and minimized in *Cerius*[2] (Molecular Simulations, 2000) and fixed at the origin. The orientation of the anion was determined using Monte Carlo simulated annealing techniques, as implemented in the *STRUCTURE_SOLVE* module of *InsightII* (Molecular Simulations, 1996). The 6–68° portion of the laboratory powder pattern was used for the structure solution. With $Z = 4$, the Mg cation also occupies a special position. The only special position that yielded a reasonable coordination geometry was $\frac{1}{4}\frac{1}{4}0$, and the position of the two

[1] Supplementary data for this paper are available from the IUCr electronic archives (Reference: BK0107). Services for accessing these data are described at the back of the journal.

Table 1
Refinement residuals.

$\Delta F+$ and $\Delta F-$ are the largest peak and the largest hole, respectively, in the difference Fourier map.

M	Mg	Mn	Fe	Co	Cu
No. of observations	19056	4160	2660	4160	5053
No. of variables	69	48	38	31	40
R_{wp}	0.1637	0.1329	0.1492	0.0557	0.0387
R_p	0.1054	0.1054	0.1201	0.0420	0.0301
$R(F^2)$	0.1174	0.0811	0.0858	0.2072	0.2056
$R(F)$	0.0702	0.0483	0.0500	0.1468	0.1966
χ^2	12.23	3.088	2.996	2.127	3.901
Normal probability plot slope	4.145	1.577	1.587	1.300	1.821
Intercept	0.326	0.106	0.128	0.016	0.037
$\Delta F+$ (e)	0.46	0.92	0.59	1.24	1.85
$\Delta F-$ (e)	−0.36	−0.42	−0.42	−1.15	−1.81

coordinated water molecules could be deduced easily. The magnesium terephthalate structure proved to be an adequate initial model for the other complexes.

2.8. Refinement

All data processing was carried out using *GSAS* (Larson & Von Dreele, 2000). The C_6H_4 core of the terephthalate anion was described as a rigid body of half-weight atoms (C—C = 1.398 Å); only the three orientation angles were refined. Soft constraints were applied to the carboxylate bond distances [C1—C11 = 1.50 (2), C11—O12 = C11—O13 = 1.28 (2) Å] and angles [C2—C1—C11 = C6—C1—C11 = 120 (3), C1—C11—O12 = C1—C11—O13 = 115 (3), O12—C11—O13 = 130 (3)°] and to the metal–oxygen bond distances. All atoms were refined isotropically; a common atomic displacement parameter U_{iso} was refined for the six C atoms of the benzene ring and the three atoms of the carboxylate group.

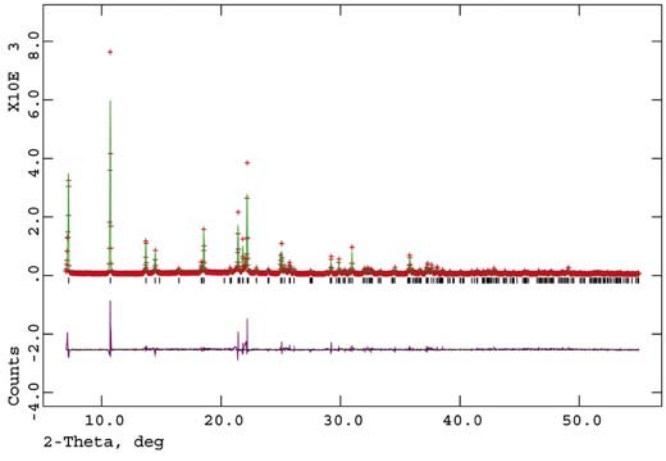

Figure 1
Observed (on beamline X3B1 at NSLS), calculated and difference patterns of magnesium terephthalate dihydrate. The crosses represent the observed data points and the solid line through them the calculated pattern. The difference pattern is plotted at the same scale as the other patterns. The large low-angle features in the difference pattern represent impurity peaks.

Included in the refinements were scale factors and the lattice parameters. The profiles were described using a pseudo-Voigt function, incorporating the Finger *et al.* (1994) description of asymmetry and the Stephens (1999) description of anisotropic strain broadening (*GSAS* profile function #4). Second- or fourth-order spherical harmonic coefficients were refined to describe the preferred orientation in the laboratory patterns. The backgrounds in the laboratory data were described using three- or six-term cosine Fourier series and the synchrotron backgrounds were modeled with six-term real-space pair correlation functions.

The final refinements yielded the residuals reported in Table 1. The largest features in the difference plots (Figs. 1–3

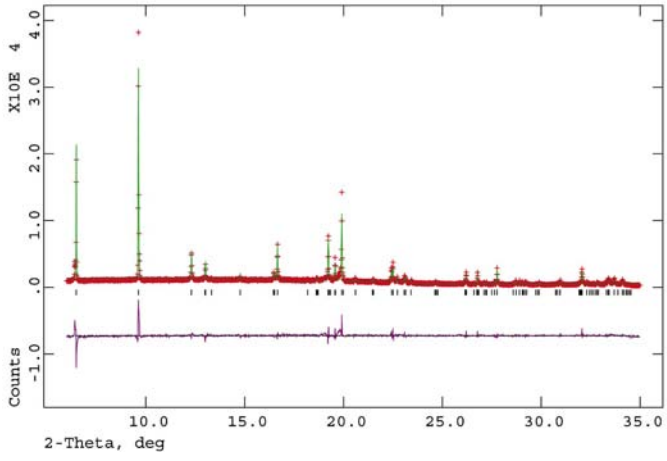

Figure 2
Observed (on beamline ID10 at APS), calculated and difference patterns of magnesium terephthalate dihydrate. The crosses represent the observed data points and the solid line through them the calculated pattern. The difference pattern is plotted at the same scale as the other patterns. The large low-angle features in the difference pattern represent impurity peaks.

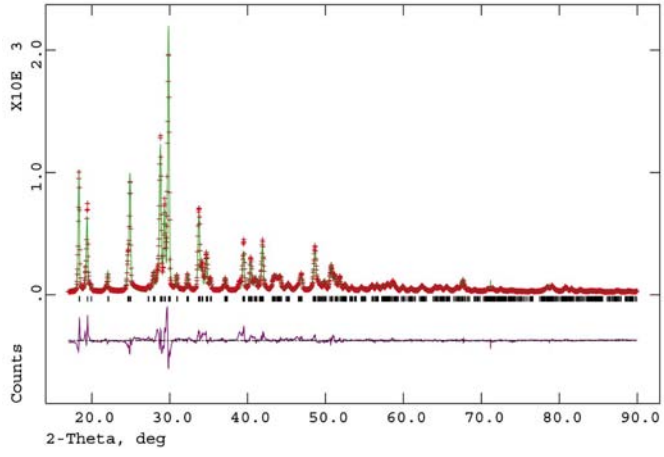

Figure 3
Observed (laboratory), calculated and difference patterns of magnesium terephthalate dihydrate. The crosses represent the observed data points and the solid line through them the calculated pattern. The difference pattern is plotted at the same scale as the other patterns.

Table 2
Refined bond distances in $M(C_8H_4O_4)(H_2O)_2$ (Å).

Quantities in italics are from the *CASTEP* geometry optimizations. Quantities in bold italics are significantly different from the observed values.

M	Mg		Mn		Fe		Co	
C11—C1	1.492 (4)	*1.484*	1.514 (3)	*1.506*	1.508 (3)	*1.510*	1.500 (3)	*1.489*
C11—O12	1.235 (4)	*1.280*	1.262 (3)	*1.298*	1.281 (3)	*1.297*	1.277 (3)	*1.289*
C11—O13	1.254 (4)	*1.259*	1.258 (3)	*1.267*	1.283 (3)	*1.266*	1.279 (3)	*1.272*
*M*14—O12 ×2	2.086 (3)	*2.125*	2.197 (3)	***2.107***	2.082 (5)	*2.087*	2.098 (4)	***2.308***
*M*14—O13 ×2	2.094 (3)	*2.057*	2.189 (3)	***2.065***	2.094 (5)	*2.000*	2.092 (4)	*2.012*
*M*14—O15 ×2	2.094 (3)	*2.129*	2.195 (2)	***1.997***	2.066 (4)	*1.965*	2.099 (3)	*1.981*
Expected *M*—O, bond valence	2.099		2.196		1.961		2.098	
Expected *M*—O, CSD	–		2.094 (79)		2.057 (51)		2.022 (83)	
M—O bond distances and overlap populations								
M	Mg		Mn		Fe		Co	
M—O12 (Å), overlap	2.125, −0.81		2.107, 0.20		2.087, 0.22		2.307, 0.12	
M—O13 (Å), overlap	2.057, −1.10		2.065, 0.24		2.000, 0.26		2.012, 0.22	
M—O15 (Å), overlap	2.129, −0.85		1.997, 0.13		1.965, 0.13		1.981, 0.11	

Table 3
Refined bond angles in $M(C_8H_4O_4)(H_2O)_2$ (°).

Quantities in italics are from the *CASTEP* geometry optimizations.

M	Mg		Mn		Fe		Co	
C1—C11—O12	120.8 (5)	*119.0*	116.2 (3)	*120.3*	114.2 (4)	*120.7*	119.1 (10)	*120.1*
C1—C11—O13	115.1 (5)	*118.0*	115.6 (3)	*118.0*	116.5 (4)	*117.3*	118.9 (8)	*117.3*
O12—C11—O13	124.0 (5)	*123.0*	127.0 (4)	*121.7*	128.4 (6)	*122.0*	116.0 (9)	*122.6*
ΣC11	359.9	*360.0*	358.8	*360.0*	359.1	*360.0*	354.0	*360.0*
O12—M14—O13	93.94 (14), 86.06 (14)	*86.4*, *93.6*	95.8, 84.2	*91.8*, *88.2*	92.5 (5), 87.5 (5)	*90.9*, *89.1*	101.1 (4), 78.9 (4)	*86.8*, *93.2*
O12—M14—O15	89.92 (15), 90.08 (15)	*87.6*, *92.4*	87.9, 92.1	*89.5*, *90.5*	84.4 (7), 95.6 (7)	*89.5*, *90.5*	89.0 (4), 91.0 (4)	*88.2*, *91.8*
O13—M14—O15	87.09 (13), 92.91 (13)	*88.2*, *91.8*	84.5, 95.5	*88.7*, *91.3*	84.0 (5), 96.0 (5)	*88.4*, *91.6*	88.0 (4), 92.0 (4)	*87.2*, *92.8*
Carboxylate torsion angles in $M(C_8H_4O_4)(H_2O)_2$								
M	Mg		Mn		Fe		Co	
C2—C1—C11—O12	18.0	*13.8*	12.0	*14.5*	10.3	*17.9*	13.7	*13.4*
C3—C1—C11—O13	14.2	*12.6*	3.0	*14.2*	7.9	*18.8*	10.2	*11.6*

Table 4
Hydrogen bonds in $M(C_8H_4O_4)(H_2O)_2$.

Quantities in italics are from the *CASTEP* geometry optimizations.

M	Mg		Mn		Fe		Co	
O15—H16···O13 (Å, °)	3.068, 147.4	*3.028*, *152.1*	2.875, 159.9	*3.258*, *135.9*	2.954, 160.4	*3.117*, *117.6*	2.834, 149.6	*3.020*, *108.9*
O15—H16···O12 (Å, °)	2.928, 136.0	*3.080*, *128.6*	3.120, 118.3	*2.963*, *145.4*	2.929, 168.8	*2.726*, *156.1*	2.986, 131.5	*2.625*, *159.4*
O15—H17···O12 (Å, °)	2.832, 172.4	*2.731*, *172.7*	2.807, 170.5	*2.918*, *166.0*	3.211, 122.2	*3.129*, *163.1*	2.871, 165.4	*2.944*, *157.2*
Overlap populations in hydrogen bonds								
M	Mg		Mn		Fe		Co	
O15—H16 overlap	0.980	0.51	0.983	0.59	0.980	0.58	1.007	0.55
H16···O13	2.179	0.03						
H16···O12	2.316	0.02	2.101	0.05	2.178	0.03	1.658	0.13
O15—H17 overlap	0.991	0.49	0.988	0.57	0.995	0.58	0.984	0.57
H17···O12	1.744	0.09	1.949	0.06	1.786	0.09	2.012	0.05

and supplementary material) represent incomplete descriptions of the profile shapes and the presence of impurities in the Mg and Co compounds. The atom coordinates and isotropic displacement coefficients are reported in the supplementary material. Bond distances and angles are reported in Tables 2 and 3. The hydrogen bonds are described in Table 4. The refined and literature coordinates for copper terephthalate trihydrate are reported in Table 5.

2.9. Quantum chemical calculations

During the refinements, the H atoms of the coordinated water molecule were placed in approximate positions based on a visual analysis of potential hydrogen bonding. The final hydrogen positions were determined by quantum chemical calculations using the Cambridge Serial Total Energy Package (*CASTEP*; Milman *et al.*, 2000) as implemented in *Cerius*[2]

Table 5
Refined atom coordinates and displacement coefficients for $Cu(C_8H_4O_4)(H_2O)_3$, space group *Pbcn*.

	Parameter	Powder	CSD JIBFUV
	a, *b*, *c* (Å)	6.8740 (3), 22.9815 (6), 6.2999 (3)	6.869 (3), 22.985 (11), 6.298 (3)
C1	$\frac{1}{2}y\,\frac{1}{4}$, *y*, U_{iso} (Å^2)	0.6701 (2), 0.048 (3)	0.6711 (1), 0.020 (2)
C2	*x*, *y*, *z*	0.4422 (11), 0.7005 (2), 0.0685 (4)	0.4349 (3), 0.7015 (1), 0.0707 (3)
C3	*x*, *y*, *z*	0.4422 (11), 0.7614 (2), 0.0685 (4)	0.4300 (3), 0.7615 (1), 0.0737 (3)
C4	$\frac{1}{2}y\,\frac{1}{4}$, *y*	0.7918 (2)	0.7915 (1)
H7	*x*, *y*, *z*, U_{iso} (Å^2)	0.4023 (19), 0.6796 (2), −0.0567 (7), 0.050	0.381 (3), 0.685 (1), −0.045 (4), 0.028 (9)
H8	*x*, *y*, *z*	0.4023 (19), 0.7823 (2), −0.0567 (7)	0.380 (4), 0.778 (1), −0.044 (5)
C11	$\frac{1}{2}y\,\frac{1}{4}$, *y*, U_{iso}, Å^2	0.6066 (4), 0.0048 (21)	0.6054 (1), 0.024 (7)
O12	*x*, *y*, *z*	0.5276 (16), 0.5805 (2), 0.4277 (9)	0.5224 (2), 0.5810 (1), 0.4268 (3)
C13	$\frac{1}{2}y\,\frac{1}{4}$, *y*	0.8590 (4)	0.8579 (1)
O14	*x*, *y*, *z*	0.4035 (14), 0.8838 (2), 0.1023 (13)	0.4021 (3), 0.8828 (1), 0.1088 (3)
O16	*x*, *y*, *z*, U_{iso} (Å^2)	0.7210 (14), 0.4824 (3), 0.3255 (16), 0.025 (5)	0.7177 (3), 0.4808 (1), 0.3060 (3), 0.020 (1)
Cu15	$\frac{1}{2}\,\frac{1}{2}\,\frac{1}{2}$, U_{iso}	0.0205 (12)	0.017 (1)
H17	*x*, *y*, *z*, U_{iso} (Å^2)	0.781, 0.505, 0.267, 0.050	0.781 (9), 0.505 (2), 0.267 (5), 0.034 (19)
H18	*x*, *y*, *z*	0.772, 0.450, 0.332	0.772 (4), 0.450 (2), 0.332 (5)
O19	$\frac{1}{2}y\,\frac{3}{4}$, *y*, U_{iso} (Å^2)	0.9353 (3), 0.0157 (38)	0.9397 (1), 0.030 (1)
H20	*x*, *y*, *z*	0.513, 0.926, 0.642	0.513 (3), 0.926 (2), 0.642 (5)

(Molecular Simulations, 2000). *CASTEP* is an *ab initio* density-functional-theory plane-wave pseudopotential code that is designed for simulation of periodic systems. Geometry optimizations were carried out using full crystallographic symmetry; the cells and the positions of the heavy atoms were fixed. Additional geometry optimization calculations (fixed experimental lattice parameters) were carried out describing the compounds as metals and using the CGA-PW91 functional and a medium basis set, with a 0.08 Å^{-1} *k*-point spacing (two-point sampling of the Brillouin zone). The default number of orbitals was increased by 10% to include some empty orbitals in the calculations. The atomic charges and bond-overlap populations were determined by the default Mulliken population analysis.

Because the transition metal salts might be expected to have unpaired electrons, additional geometry optimizations of a more sophisticated nature were carried out using spin-polarized functionals. The geometries were essentially identical to the results reported here and are not discussed further. Although such calculations can be carried out in *CASTEP*, it lacks the spin terms necessary to describe spin–spin interactions; *CASTEP* is thus not well suited to calculating magnetic properties. Cobalt terephthalate dihydrate has recently been reported to be paramagnetic (Kurmoo *et al.*, 2001). The differences between the experimental and fully optimized geometries of the transition metal salts probably result from this lack of spin–spin interactions.

The calculated powder patterns of these compounds have been submitted to the International Centre for Diffraction Data for inclusion in future releases of the Powder Diffraction File.

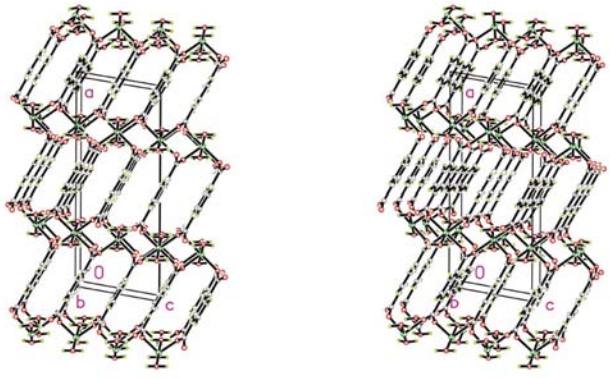

Figure 4
The crystal structure of $M(C_8H_4O_4)(H_2O)_2$ viewed down the *b* axis.

3. Results and discussion

3.1. Mg, Mn, Fe and Co(II) terephthalate dihydrates

The structure consists of alternating layers (perpendicular to *a*) of terephthalate anions and octahedrally coordinated metal cations (Fig. 4). The octahedra are isolated; the equatorial coordination consists of four terephthalate O atoms and there are two axial water molecules (Fig. 5). The cation valences, calculated from the sums of bond valences (Brese &

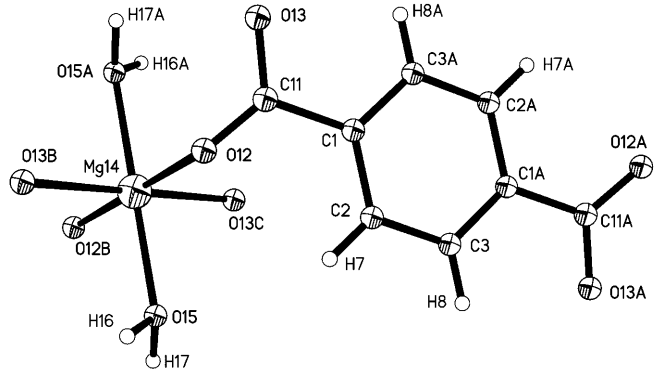

Figure 5
The metal coordination sphere and the terephthalate anion in magnesium terephthalate dihydrate with the atom-numbering scheme. Heavy atoms are represented by 50% probability spheroids and H atoms by circles of arbitrary radius.

O′Keefe, 1991), are 2.04, 2.02, 2.35 and 1.97 for Mg, Mn, Fe and Co, respectively. The lower stability of the Fe complex is consistent with its high valence.

The bond distances fall within the normal ranges (they were subject to soft constraints). A search of the Cambridge Structural Database (Allen & Kennard, 1993) for aromatic carboxylates that bridge two metal atoms yielded reasonable populations for Mn, Fe and Co (Table 2) but none for Mg. Both these values and those calculated using the bond-valence formalism can be used to assess the refined M—O distances. Both Mn—carboxylate and Co—carboxylate distances are shorter than those of general MO_6 coordination spheres, while the Fe—carboxylate distances are larger. The deviations of the O—M—O angles from the ideal octahedral angles are small, except for Co, in which the equatorial angles are 101° and 79°.

The bond distances and angles of the carboxylate groups of the terephthalate anions were subject to soft constraints, so they fall within the normal ranges. (The soft constraints accounted for only a few percent of the final reduced χ^2.) The C—O bonds are equal in length and resonant; because they bridge two metal atoms, this is reasonable. The carboxylate in the Co complex is decidedly non-planar (the sum of the angles around C11 is 354.0°).

None of the terephthalate anions are completely planar; the carboxylates are rotated approximately 10° out of the ring plane. As we have noted, aromatic carboxylates are more flexible than is commonly believed. These rotations result in only a small energy penalty (∼3 kJ mol^{-1}; Kaduk & Golab, 1999) and result in coordination geometries that are more favorable.

Both water-molecule H atoms participate in normal-strength hydrogen bonds to carboxylate O atoms. Visualization of the structures suggests two potential hydrogen bonds involving each H atom; quantum calculations (below) were necessary to gain insight into the hydrogen bonding.

The stacking of the aromatic rings is relatively 'tight'; the shortest intermolecular C···C and C···H distances fall in the range 3.2–3.3 Å. The angle between successive ring planes in the stack is 8.0° in the Mg complex. The densities of these complexes are not exceptionally high (Mg = 1.709, Mn = 1.878, Fe = 1.937, Co = 1.996 g ml^{-1}) and the 'side-to-side' packing of the terephthalates is relatively 'loose' (supplementary material). There is a significant volume that could be occupied by probes of 0.8–1.0 Å radius. Apparently, the coordination interactions are more important than the packing of the aromatic anions in determining the crystal structure. The terephthalate packing does not fit the pattern of aromatic hydrocarbons, in contrast to that in terephthalates of monopositive cations (Kaduk, 2000).

The structure of these compounds differs from those of copper and zinc terephthalate dihydrates. In copper terephthalate dihydrate (Deakin *et al.*, 1999), the metal is five-coordinate (square pyramidal) and is coordinated to two monodentate carboxyls, two bridging water molecules and one monodentate water molecule. In zinc terephthalate dihydrate (Guilera & Steed, 1999), the zinc coordination is tetrahedral and each carboxyl is monodentate. Just as in the current structures, each water-molecule H atom participates in a hydrogen bond in these two structures.

3.2. Comparison of refined and optimized structures and bonding in the complexes

In general, the agreement between the Rietveld-refined and the *CASTEP*-optimized structures is good. The weighted r.m.s. deviations between the atom positions are 0.054 (Mg), 0.154 (Mn), 0.202 (Fe) and 0.204 Å (Co) for the 12 atoms of the asymmetric unit. The agreement of the deviations among the non-H atoms is better: 0.030 (Mg), 0.107 (Mn), 0.149 (Fe) and 0.157 Å (Co). Because the Mg structure is by far the best determined (the refinement included two synchrotron powder patterns) and this compound contains no unpaired electrons, this trend is reasonable. Since the Mn, Fe and Co structures were refined using only laboratory data, the optimized structures for these metals may be *better* than the experimental structures. In the optimized Mn structure, the Mn—O bond distances are much closer to those expected from an analysis of Mn—carboxylate distances in the CSD (Table 2). In the optimized Co structure, the Co—O12 distance has become very long (2.308 Å). In all four optimized structures, the carboxylate groups are planar and the O—M—O angles are closer to the ideal octahedral values; the optimized structures are more chemically reasonable.

All of the bond distances, angles, charges and overlap populations in the terephthalate ions indicate that the terephthalates in these four compounds are essentially identical; the differences lie in the metal–terephthalate and hydrogen bonding.

Both the atomic charges (Fig. 6) and the M—O bond-overlap populations (Fig. 7 and Table 2) indicate that, despite the fact that these compounds are isostructural, the metal–terephthalate bonding is different. The bonding in the magnesium complex is essentially ionic, while the M—O bonds in the Mn, Fe and Co complexes have significant covalent character. Detailed analysis of the density of states plots (Fig. 8) reveals significant overlap of metal *d*-orbitals with carboxylate oxygen *p*-states in the Mn, Fe and Co

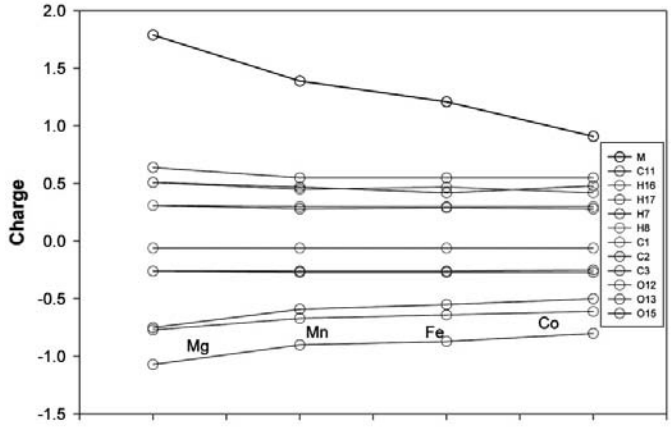

Figure 6
The *CASTEP*-calculated atomic charges in $M(C_8H_4O_4)(H_2O)_2$.

complexes. The density of states in the Co complex differs significantly from those of the Mn and Fe compounds; the bonding would be expected to be different. Visualization of the individual molecular orbitals provides additional insight into the metal–oxygen bonding.

Visualization of the structure (Fig. 9) suggests two plausible potential hydrogen bonds between each water-molecule H atom and a carboxylate O atom (O12 or O13). The quantum calculations demonstrate, however, that both H16 and H17 form hydrogen bonds to O12 in the Mn, Fe and Co complexes (Table 4). In magnesium terephthalate dihydrate, H16 forms hydrogen bonds to both O12 and O13. The carboxyl O atom O13 does not serve as a hydrogen-bond acceptor in the transition metal complexes. Although O13 is less negatively charged than O12 (Fig. 6), the hydrogen bonds are clearly more than just electrostatic interactions. Other than the covalent bonds, the only other positive overlap populations represent the hydrogen bonds (Table 4). The overlap population of the water-molecule covalent O—H bonds varies from 0.5–0.6 electrons in these complexes. Because such a bond has a dissociation energy of ~490 kJ mol^{-1}, even the overlap populations of 0.03–0.10 electrons in the O···H hydrogen bonds correspond to considerable attraction energy. In the Co complex, the H16···O12 hydrogen bond is much stronger than the others, correlated to the long Co—O12 distance in this complex. The coordination and hydrogen-bond interactions are the most important in determining the structures of these complexes.

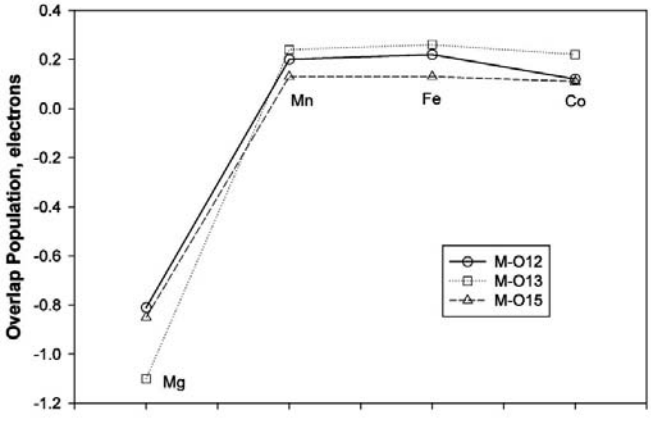

Figure 7
The M—O bond-overlap populations (*CASTEP*) in $M(C_8H_4O_4)(H_2O)_2$.

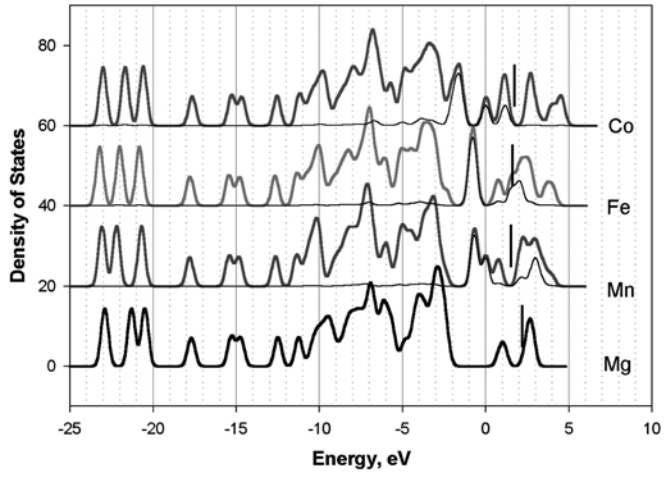

Figure 8
Density of states in $M(C_8H_4O_4)(H_2O)_2$. The heavy lines represent the total density of states and the thin lines the *d*-state density. The vertical bars indicate the Fermi levels.

3.3. Copper(II) terephthalate trihydrate

The crystal structure of *catena*-[diaqua(μ^2-terephthalato-*O*,*O*′)copper(II) dihydrate], or copper terephthalate trihydrate, has been reported (Cueto *et al.*, 1991; Deakin *et al.*, 1999) as a high-quality single-crystal refinement. The structure is very different to those of the other divalent first-row transition metals, presumably the result of Jahn–Teller effects.

In this structure (Fig. 10), the Cu(II) coordination is square planar; two additional water molecules (coordinated to an adjacent Cu) lie 2.48 Å away on axial positions. Only one end of the terephthalate anion is coordinated to the Cu; it bridges two Cu cations to form zigzag chains parallel to the *c* axis in this orthorhombic structure. The other carboxylate forms strong hydrogen bonds to coordinated water molecules.

Comparison of the reported single-crystal structure with a new refinement based on powder data collected using the same conditions as for the Mg, Mn, Fe and Co salts (Fig. 11) provides an opportunity to assess the accuracy and precision that can be expected from structures of aromatic carboxylates

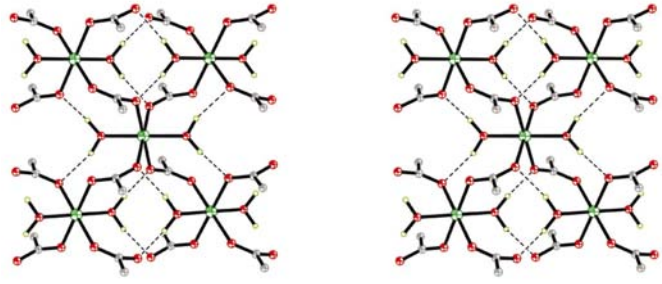

Figure 9
The hydrogen-bonding network in $M(C_8H_4O_4)(H_2O)_2$.

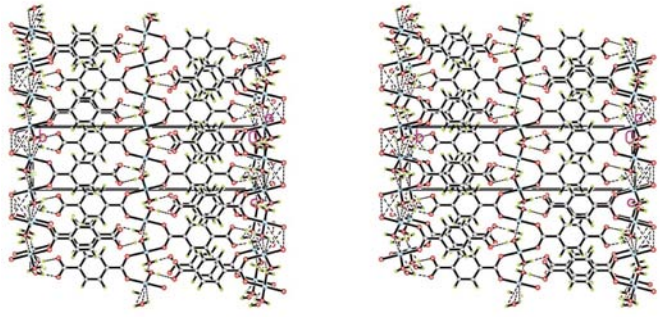

Figure 10
The crystal structure of copper terephthalate trihydrate.

determined using X-ray powder data (Tables 5 and 6). As expected, the lattice parameters are determined more precisely using high-quality powder data. The estimated standard uncertainties on the coordinates from the Rietveld refinement are a factor of three larger than those from the single-crystal refinement; the slope of the normal probability plot indicates that these standard uncertainties are underestimated by almost a factor of two. The displacement coefficients are less well determined using a single laboratory X-ray powder data set.

Table 6
Bond distances (Å) and angles (°) in $Cu(C_8H_4O_4)(H_2O)_3$.

All of the bond distances and the carboxyl bond angles were subject to restraints (soft constraints).

Parameter	Powder	CSD JIBFUV	Parameter	Powder	CSD JIBFUV
C11—C1	1.460 (8)	1.510	C1—C11—O12	117.9 (5)	116.5
C11—O12	1.284 (5)	1.256	O12—C11—O12	124.3 (9)	127.0
C13—C4	1.546 (9)	1.526	C4—C12—O14	116.5 (5)	117.2
C13—O14	1.276 (6)	1.253	O14—C13—O14	127.0 (11)	125.7
Cu15—O12 ×2	1.914 (4)	1.925 (2)	O12—Cu15—O16	89.4 (4)	89.6 (1)
Cu15—O16 ×2	1.918 (7)	1.981 (2)	O12—Cu15—O16	90.6 (4)	90.4 (1)

The average difference between the bond distances in the two structures is 0.03 Å and the average difference in bond angles is only 1.1°. (These differences include all distances and angles – both constrained and unconstrained. The restraints contributed only 0.6% to the final reduced χ^2.) The largest difference is in the Cu15—O16 distance to the coordinated water molecule. This accuracy and precision is comparable to that observed in a similar comparison of cobalt acetate tetrahydrate refinements (Kaduk & Partenheimer, 1997) and demonstrates that sufficient accuracy and precision to answer chemical questions can reasonably be expected from Rietveld refinements. These metal terephthalate dihydrate structures thus form a reasonable platform from which to build knowledge of other metal terephthalate structures.

The iron and cobalt terephthalate samples were provided by T. G. Carlstedt and B. J. Huggins, respectively. The author wishes to thank Nadia Leyarovska, Holger Tostmann, Jeremy Kropf and Peter Stephens for their assistance in the synchrotron data collections. Keith Glassford of Accelrys provided excellent instruction in how to carry out and interpret the quantum calculations. The MRCAT beamline at the Advanced Photon Source was supported by the US Department of Energy under grant number DE-FG02-00ER-45811. The SUNY PRT beamline at NSLS is supported by the Division of Basic Energy Sciences of the US Department of Energy (grant DE-FG02-86ER-45231).

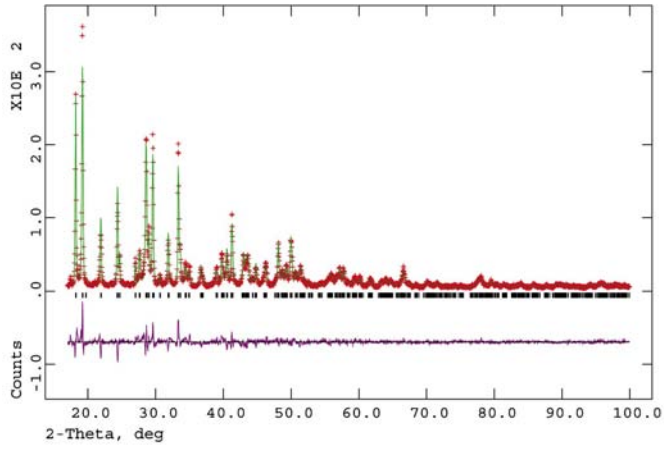

Figure 11
Observed, calculated and difference patterns of copper terephthalate trihydrate.

References

Allen, F. H. & Kennard, O. (1993). *Chem. Des. Autom. News*, **8**, 31–37.
Barker, R. S. & Saffer, A. (1958). US Patent 2 833 816.
Brese, N. E. & O'Keefe, M. (1991). *Acta Cryst.* B**47**, 192–197.
Brzyska, W. (1971). *Ann. Univ. Mariae Curie-Sklodowska Sect. AA*, **26**/**27**, 105–111.
Cueto, S., Gramlich, V., Petter, W. & Rys, P. (1991). *Acta Cryst.* C**47**, 75–78.
Deakin, L., Arif, A. M. & Miller, J. S. (1999). *Inorg. Chem.* **38**, 5072–5077.
Ebara, N. & Furuyama, S. (1973). *Sci. Pap. Collect. Gen. Educ. Univ. Tokyo*, **23**, 29–33.
Finger, L. W., Cox, D. E. & Jephcoat, A. P. (1994). *J. Appl. Cryst.* **27**, 892–900.
Furuyama, S. & Ebara, N. (1967). *Sci. Pap. Collect. Gen. Educ. Univ. Tokyo*, **17**, 81–88.
Groeneman, R. H. & Atwood, J. L. (1999). *Cryst. Eng.* **2**, 241–249.
Guilera, G. & Steed, J. W. (1999). *Chem. Commun.* pp. 1563–1564.
Kaduk, J. A. (2000). *Acta Cryst.* B**56**, 474–485.
Kaduk, J. A. & Golab, J. T. (1999). *Acta Cryst.* B**55**, 85–94.
Kaduk, J. A. & Partenheimer, W. (1997). *Powder Diff.* **12**, 27–39.
Kurmoo, M., Kumagai, H., Green, M. A., Lovett, B. W., Blundell, S. J., Ardavan, A. & Singleton, J. (2001). *J. Solid State Chem.* **159**, 343–351.
Larson, A. C. & Von Dreele, R. B. (2000). *GSAS*. Los Alamos National Laboratory, Los Alamos, NM, USA.
Matsuzaki, T. & Iitaka, Y. (1972). *Acta Cryst.* B**28**, 1977–1981.
Meyer, D. H. (1971). US Patent 3 584 039.
Michaelides, O. A., Tsaousis, D., Skoulika, S., Raptopoulou, C. P. & Terzis, A. (1998). *Acta Cryst.* B**54**, 657–662.
Milman, V., Winkler, B., White, J. A., Pickard, C. J., Payne, M. C., Akhmatskaya, E. V. & Nobes, R. H. (2000). *Int. J. Quantum Chem.* **77**, 895–910.
Miyakubo, K., Takeda, S. & Nakamura, N. (1994). *Bull. Chem. Soc. Jpn*, **67**, 2301–2303.
Molecular Simulations (1996). *InsightII.* Version 4.0. Molecular Simulations, 9685 Scranton Road, San Diego, CA 92121, USA.
Molecular Simulations (2000). *Cerius*^{2}. Version 4.2MS. Molecular Simulations, 9685 Scranton Road, San Diego, CA 92121, USA.
Partenheimer, W. (1995). *Chem. Ind.* **62**, 307–317.
Reineke, T. M., Eddaoudi, M., Fehr, M., Kelley, D. & Yaghi, O. M. (1999). *J. Am. Chem. Soc.* **121**, 1651–1657.
Sherif, F. G. (1970). *Ind. Eng. Chem. Prod. Res. Dev.* **9**, 408–412.
Stephens, P. W. (1999). *J. Appl. Cryst.* **32**, 281–289.